Feature-based Analysis of a Multi-Parameter Flow Simulation

Tino Weinkauf* Zuse Institute Berlin
Jan Sahner* Zuse Institute Berlin
Bert Günther† Berlin University of Technology
Holger Theisel‡ Magdeburg University
Hans-Christian Hege* Zuse Institute Berlin
Frank Thiele† Berlin University of Technology

Abstract

In our work we examine a high-dimensional, massive flow data set around an airfoil using a topology-based vortex analysis. The 3D time-dependent flow depends on two additional parameters which are introduced by an active flow control technique aiming at increasing the lift by periodic blowing and suction. In particular, we study the influence of the actuation parameters frequency and intensity of air injection and show how our vortex analysis helps in understanding the underlying physics.

1 Introduction

Computing power increases constantly. While the fastest supercomputer in 1993 had a performance of 59.7 GFlop/s, the fastest installation in 2007 reached 280.6 TFlop/s [MSDS]. This is an increase by a factor of 4700. As of this writing, the petascale era is already approaching. Along with the computing power, the size and complexity of simulation results is increasing as well. In many cases the simulated data sets are at least four-dimensional, e.g. with three spatial dimensions and time.

This paper deals with the analysis of a flow data set which incorporates two additional parameters. These parameters are introduced by a periodic excitation of the flow around an airfoil which aims at increasing the lift. This active flow control technique employs an unsteady wall jet located near the leading edge of the flap to excite the flow and thus provoke either delay of separation or reattachment. Important parameters of this excitation are *frequency* and *intensity* of air injection. In our work we study 23 different parameter combinations and aim at finding the one with the highest lift. Most important, we want to understand the underlying physics and explain *why* the lift is higher for a certain parameter set than for another. This can guide in finding new excitation strategies.

Each parameter combination is a 3D time-dependent flow field with 200 time steps. The grid consists of 1.3 million cells. This totals in over 200 GB of data. Due to the sheer size

* {weinkauf, sahner, hege}@zib.de, Department Visualization and Data Analysis, D-14195 Berlin, Germany
† {bert.guenther, frank.thiele}@cfd.tu-berlin.de, Institute of Fluid Mechanics and Engineering Acoustics, Müller–Breslau–Straße 8, D-10623 Berlin, Germany
‡ theisel@isg.cs.uni-magdeburg.de, Department of Simulation and Graphics, D-39106 Magdeburg, Germany

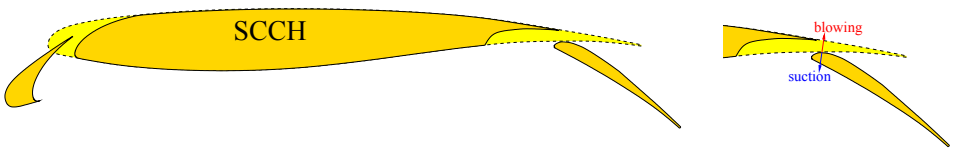

(a) Sketch of the SCCH high-lift-configuration. (b) Excitation at the flap.

Figure 1: SCCH Wing Model and periodic excitation by blowing and suction.

of the data set alone, it is favorable if not necessary to automate at least parts of the analysis. A way to achieve this is by extracting features. In this paper, we study the vortex structures of the flow since they indicate the degree and success of the induced perturbation.
In section 2 we discuss the simulation part of our work. In section 3 we present our feature-based analysis methods. The different parameter variations are studied in section 4 and conclusions are drawn in section 5.

2 Simulation and Flow Control

Engineers aim at controlling flow with active and passive mechanisms. Passive methods contain effects caused by adequate profiling or by self-triggered processes of the flow. In contrast, active methods are characterized by excitation mechanisms that insert external energy into the flow.
Passive methods have been well-investigated in the last decades and have been integrated in scores of technical applications in the form of vortex generators as well as Gurney flaps [SGT04]. Today, the majority of research is focused on concepts with active flow control.
A large number of experimental and numerical studies have shown the general effectiveness of active flow control for single airfoils. In most investigations, leading edge suction is applied to delay transition [MCML89]; nonetheless, jet flaps are also employed for lift increase and manoeuvering. Surface suction/blowing can be used to rapidly change lift and drag on rotary wing aircraft [HJ97].
Overviews of active flow control are given by Wygnanski and Gad-el-Hak [Wyg04, GeH01].

2.1 Wing Model

The wing used for the simulations is the *SCCH* (**S**wept **C**onstant **C**hord **H**alf model) high-lift configuration that has already been used for several experimental studies targeting passive flow and noise control concepts [Koo05, KKE05], see Figure 2.1. The problem is modeled as an infinite swept wing (2.5D) in order to reduce the computational domain to a single spanwise segment of the configuration. This simulation hence incorporates the three-dimensional effects generated by the sweep but neglects root or Tipp effects. The typical three-component setup consists of a main airfoil equipped with deployed slat and

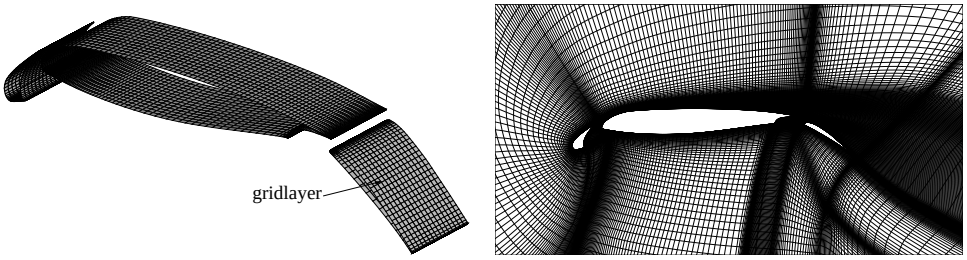

(a) surface mesh of the computed wing segment (b) 2-dimensional mesh near the configuration

Figure 2: Computational mesh

flap, see (figure 1a). All profiles have blunt trailing edges. The flap is situated at a fixed position underneath the trailing edge. The angle of attack is fixed at 6 degrees for the whole configuration, which is situated in the typical range of approach for civil aircraft.
In all numerical investigations the freestream velocity corresponds to a Reynolds number of $Re = 10^6$, based on the chord of the clean configuration (with retracted high-lift devices). This high Reynolds number is chosen to demonstrate the relevance to industrial applications.

2.2 Numerical Method

The numerical method applied is based on a three-dimensional incompressible finite-volume scheme for solution of the Reynolds-averaged Navier-Stokes equations. The three-dimensional method is fully implicit and of second order accuracy in space and time. Based on the SIMPLE pressure correction algorithm, a co-located storage arrangement for all quantities is applied. Convective fluxes are approximated by TVD. In previous investigations of unsteady turbulent flows, the LLR k-ω turbulence model by Rung [RT96] exhibited the best performance.

2.3 Computational Mesh

Figure 2 shows the mesh around the slat, the main airfoil and the flap. The dimensions of the computational domain are 15 chords forward, above and below the configuration and 25 chords behind. Figure 2b shows the two-dimensional mesh around the entire configuration. The two-dimensional computational c-type mesh consists of 90,000 cells in total. The non-dimensional wall distance of the first cell center remains below $Y^+ = 1$ on the complete surface.
The three-dimensional grid is based on an expansion of the two-dimensional mesh into the third direction. For consideration of an infinite swept wing 16 layers of the two-dimensional mesh are combined to resolve a three-dimensional wing section by 1,300,000 cells in total (figure 2a) for each of the 202 time steps. The infinite span is simulated by means of periodic boundary conditions.

2.4 Time Step Size

From initial numerical investigations of the configuration without excitation, characteristics of the unsteady behavior are already known. A separate study of the influence of time step size indicated that a typical time step of $\Delta t = 4.2 \times 10^{-3}\, c/u_\infty$ is sufficient to obtain results independent of the temporal resolution. All computations presented here are based on $\Delta t = 2.1 \times 10^{-3}\, c/u_\infty$, which allows a resolution of around 202 time steps per oscillation cycle for a non-dimensional oscillating frequency of $F^+ = 0.6$.

2.5 Boundary Conditions

At the wind tunnel entry all flow quantities including the velocity components and turbulent properties are prescribed. The level of turbulence at the inflow is set to $Tu = \frac{1}{u_\infty}(\frac{2}{3}k)^{1/2} = 0.1\%$ and the turbulent viscosity $\mu_t/\mu = 0.1$. At the outflow a convective boundary condition is used that allows unsteady flow structures to be transported outside the domain. The complete airfoil and flap surface is modeled as a non-slip boundary condition. As the resolution is very fine, a low-Re formulation is applied. The wind tunnel walls are neglected in the far field.

2.6 Excitation Mechanism

To model the excitation apparatus, a periodic suction/blowing type boundary condition is used. The perturbation to the flow field is introduced through the inlet velocity on a small wall section representing the excitation slot:

$$u_{exc}(t) = u_a \cdot \sin\left[2\pi \cdot \frac{c}{c_k} \cdot F^+ \cdot \tau\right] \tag{1}$$

$$\text{with} \qquad u_a = u_\infty \sqrt{\frac{c}{H}\, C_\mu}\,, \qquad F^+ = f_{per} \cdot \frac{c_k}{u_\infty}\,, \qquad \tau = t \cdot \frac{c}{u_\infty}$$

where c is the clean chord length, c_k the flap length, u_a is the amplitude velocity of the perturbation oscillation, F^+ is the non-dimensional perturbation frequency, τ is the dimensionless time given in convective units of the whole configuration, H is the slot width between main airfoil and flap ($H = 0.00186\ c_k$) and C_μ is the non-dimensional steady momentum blowing coefficient. The oscillating jet is emitted perpendicular to the wall segment of the excitation slot, and is located at 6% chord behind the flap leading edge (figure 1b).

3 Methods for the Feature-based Vortex Analysis

In the following we present our analysis approach which is based on the examination of vortex structures. Vortices play a major role in all flow applications due to their wanted or unwanted effects on the flow. In turbomachinery design, certain types of vortices reduce efficiency, whereas in burning chambers, vortices have to be controlled to achieve optimal

mixing of oxygen and fuel. In our case of the flow around an airfoil, the manipulation of small shear-layer vortex structures is known to increase the desired lift and to reduce the parasitic drag.

3.1 Introduction to Feature Extraction

The data to be analyzed in this paper consists of three spatial dimensions, the time dimension, and two parameter dimensions. While the latter have been covered sparsely, it is still a complex data set. The human brain has the ability to grasp primarily three dimensions and the current hardware has only limited capabilities of displaying them. Hence, only parts of the massive and complex simulation results can be visualized (or otherwise presented to the examiner) at once.
Therefore, we choose an analysis technique which allows us to condense the flow to its structural vortex skeleton by means of feature extraction, which reduces the amount of data to a small set of geometric objects. Furthermore, a quantification of the extracted features allows to build up a feature hierarchy leading to even further simplified representations by e.g. filtering out the less important features.
Feature extraction is used to automatically find interesting parts in the data. This can guide the user in the manual exploration of a data set. It allows to concentrate on certain aspects of the data like the vortex structures. Furthermore, is easily automated and therefore, it is perfectly fitted for batch jobs on supercomputers. The resulting feature set is usually small enough to be handled and displayed interactively with commodity hardware. Hence, the time needed by the user is reduced since parts of the analysis are automated and the manual part is interactive. In contrast to most other visualization methods, feature extraction techniques usually depend on less parameters or even no parameters at all. Hence, the interpretation of the results depends less on a user-defined parametrization (e.g. isovalue, transfer function).

3.2 Vortex Analysis using Extremum Lines

In the following we describe our approach to extracting vortex structures. This is done by considering extremum lines (ridges or valleys) of Galilean invariant vortex region quantities. The method is based on a topological analysis and uses first order derivatives of the examined scalar field only.
While Post et al. [PVH$^+$02] and Peikert et al. [PR99] give a thorough overview of algorithms for the treatment of vortical structures, a short introduction is given here. They can be classified in two major categories:

- *Vortex region detection* is based on scalar quantities that are used to define a vortex as a spatial region where the quantity exhibits a certain value range. We refer to them as *vortex region quantities*. Examples of this are regions of high vorticity magnitude, negative λ_2-criterion [JH95], or positive Q-criterion [Hun87]. In general, these measures are Galilean invariant (e.g., they are invariant under translational changes of the reference frame). This is due to the fact that their computation involves only derivatives of the vector field. Isosurfaces or volume rendering are common approaches for

vortex region quantity	vortex range	vortex core type
p	$[0, \infty)$	valley
$\|\omega\|$	$(0, \infty)$	ridge
Q	$(0, \infty)$	ridge
λ_2	$(-\infty, 0)$	valley

Table 1: Vortex region quantities pressure p, vorticity ω, Q-criterion and λ_2 criterion with the value range in which they indicate vortices. Vortex cores according to definition 1 are either ridges or valleys as shown in the third column.

visualizing these quantities, which require the choice of thresholds and appropriate isovalues or transfer functions. This can become a difficult task for some settings.

- *Vortex core line extraction* aims at extracting line type features that are regarded as centers of vortices. Different approaches exist, e.g. cores of swirling motion [SH95, RP98, PR99, WSTH07], vorticity lines corrected towards pressure minima [BS95] or λ_2 minima [SRE05], or lines of extremal scalar value [MK97, SWH05a, SWTH07]. The extraction of such lines is parameter free in the sense that their definition does not refer to a range of values. This eliminates the need of choosing certain thresholds.

Table 1 lists a number of vortex region quantities. Besides their Galilean invariance, they have in common that vortex activity is locally maximal where the scalar field becomes locally extremal [Hun87, JH95]. Hence, the core line of a vortex can be defined as an extremum line of such a Galilean invariant vortex region quantity. We give the following:

Definition 1 *Let s be a Galilean invariant vortex region quantity. In regions where s identifies a vortex, a* **Galilean invariant vortex core line** *with respect to s is defined as a*

$$\left.\begin{matrix}\textit{ridge line}\\ \textit{valley line}\end{matrix}\right\} \textit{ of } s \textit{ if } \begin{cases}\textit{large}\\ \textit{small}\end{cases}$$

values of s indicate a vortex.

Table 1 also shows whether so-defined vortex core lines are ridges or valleys of the respective quantity. A vortex analysis based on definition 1 has a number of advantages:

- In contrast to an isosurface extraction or volume rendering of the respective quantity, the extraction of extremum lines is parameter free in the sense that their definition does not refer to a range of values. This eliminates the need of choosing certain thresholds or transfer functions. In other words, it objectifies the analysis and the extraction can easily be applied without user interaction, for instance as a batch job prior to visualization or during the simulation. See figure 3.
- Extremum lines correctly identify location and extent of the vortices in contrast to isosurfaces, which may break up along vortices or may contain several independent vortices. See figure 3.

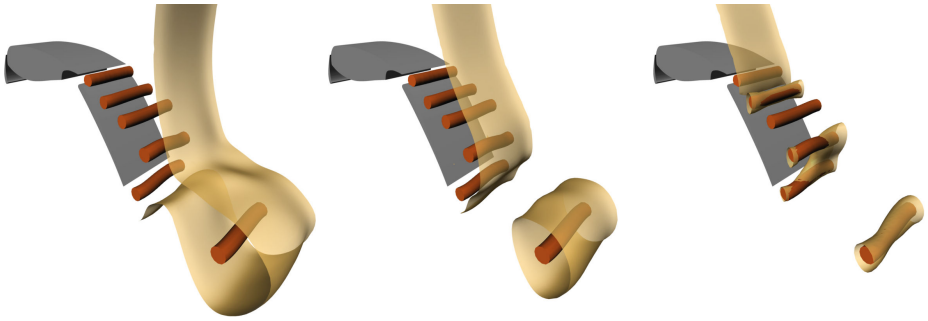

Figure 3: Minimal lines of pressure (red) and pressure isosurface (yellow). Shown is the same time step, but three different isovalues for the isosurface extraction. A precise vortex analysis using isosurfaces is difficult since they may break up along vortices or may contain several independent vortices. In contrast to this, extremum lines correctly identify location and extent of the vortices.

- In contrast to a volume rendering, extremum lines allow for a quantitative analysis since they are well-defined geometric objects. Hence, several characteristics can be *measured*: the extent of a vortex, its distance to the body (e.g. an airfoil), its temporal evolution, its life time, and much more. This gives rise to a statistical analysis.
- In contrast to the cores of swirling motion [SH95, PR99, WSTH07], the core lines based on definition 1 are Galilean invariant.

Several notions of extremum lines have been developed in the literature [Ebe96, SWH05a, SWTH07]. Here, we use the method of Sahner et al. [SWTH07] which extracts such structures using topology, i.e., the extremum lines are a part of the topological skeleton of the examined vortex region quantity.
The topology of a 2D scalar field is analogous to the watershed lines of a 2D terrain: at certain line structures, rain water separates in the sense that nearby water collects in different valleys. Those maximum lines partition the domain into valleys, within which all the water flows towards the same minimum. Similarly, the domain is partitioned into hills separated by minimal lines called watercourses. On hills all water runs down from one maximum.
The generalization to 3D is straightforward. Here the watersheds are surfaces, and additional one-dimensional separatrices come into play, which are *lines of minimal/maximal scalar value*. Under the assumption that the examined scalar field is an indicator of vortex activity (e.g. as listed in table 1) these lines denote vortex core lines following definition 1.

3.3 Extraction

The topological skeleton of a scalar field is called Morse-Smale complex [Mil63]. A number of different extraction strategies can be applied [RM00, EHNP03]. If the scalar function is differentiable, its topology can be obtained as the *vector field topology* of its gradient and

corresponding extraction schemes can be applied [HH91, TWHS03]. We choose this approach, since the results of this scheme are smooth connected lines. We refer the reader to Sahner et al. [SWTH07] for a discussion of different extraction schemes in this context.
The topological analysis starts with the extraction of so-called critical points. Considering a vector field $\mathbf{v}(\mathbf{x})$ (in our case, the gradient of a vortex region quantity), an isolated *critical point* $\mathbf{x}_0$ is given by

$$\mathbf{v}(\mathbf{x}_0) = \mathbf{0} \quad \text{with} \quad \mathbf{v}(\mathbf{x}_0 \pm \boldsymbol{\epsilon}) \neq \mathbf{0} \quad \text{for some } \epsilon > 0. \tag{2}$$

This means that $\mathbf{v}$ is zero at the critical point, but non-zero in a certain neighborhood.
In order to find these isolated zeros, we use the following scheme: we check whether at least one component of the field is positive/negative at *all* corners of a cell. If so, a zero cannot appear in that cell. Otherwise, we recursively subdivide the cell until a certain threshold is reached. This component-wise change-of-sign test is a necessary condition for a zero inside a (bi-/tri-)linearly interpolated grid cell. This is very fast to compute and a number of real word data sets (including the ones analyzed in section 4) are already given as piecewise trilinear fields on regular grids: here, our criterion can readily be applied to the original grid and zeros cannot be missed.
Critical points are characterized and classified by the behavior of the tangent curves around it. As shown in [HH91], a first order Taylor expansion of the flow around $\mathbf{x}_0$ suffices to completely classify it. This is done by an eigenvalue/eigenvector analysis of the Jacobian $\mathbf{J}(\mathbf{x}_0)$. Let λ_i be the eigenvalues of $\mathbf{J}(\mathbf{x}_0)$ which are always real since we restrict ourselves to gradient fields. Let them be ordered such that $\lambda_{i-1} \leq \lambda_i$. Furthermore, let $\mathbf{e}_i$ be the corresponding eigenvectors. The sign of an eigenvalue λ_i denotes – together with the corresponding eigenvector $\mathbf{e}_i$ – the flow direction: positive values represent an *outflow* and negative values an *inflow* behavior. Depending on the sign of λ_i we get the following classification of first-order critical points in 3D vector fields:

Sources:	$0<\lambda_1 \leq\lambda_2 \leq\lambda_3$
Repelling saddles:	$\lambda_1 < 0<\lambda_2 \leq\lambda_3$
Attracting saddles:	$\lambda_1 \leq\lambda_2 < 0<\lambda_3$
Sinks:	$\lambda_1 \leq\lambda_2 \leq\lambda_3 < 0$

Sources and sinks consist of complete outflow/inflow, while saddles have a mixture of both. A repelling saddle has one direction of inflow behavior (called *inflow direction*) and a plane in which a 2D outflow behavior occurs (called *outflow plane*). Similar to this, an attracting saddle consists of an *outflow direction* and an *inflow plane*.
Note that the elements of the topological skeletons of a scalar field s and its gradient vector field $\mathbf{v} = \nabla s$ correspond to each other as shown in table 2. A minimum of s is a source of $\mathbf{v}$, i.e., scalar values are increasing along gradient curves started close to a minimum. Similarly, they are decreasing along gradient curves started near a maximum. Certain gradient curves started close to saddle points have such a distinct behavior, too. They are part of the so-called separatrices, which are stream lines or stream surfaces separating regions of different flow behavior. In our case of a gradient vector field, these lines and surfaces denote extremum lines and surfaces. These extremum lines are the centers of vortices. They can

scalar field s	gradient vector field $\mathbf{v} = \nabla s$
minimum	source
1-saddle	repelling saddle
2-saddle	attracting saddle
maximum	sink
maximum line	unstable 1D manifold, repelling separation line
minimum line	stable 1D manifold, attracting separation line
maximum surface	unstable 2D manifold, repelling separation surface
minimum surface	stable 2D manifold, attracting separation surface

Table 2: Terminology of the topological elements in 3D scalar and vector fields.

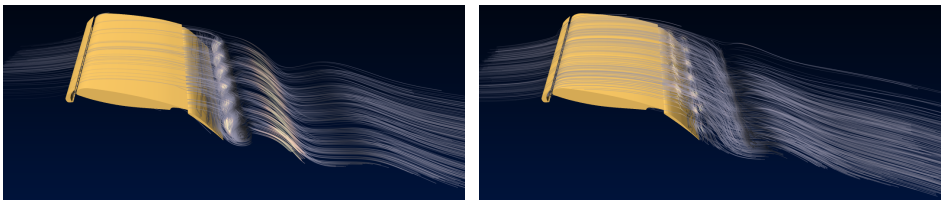

(a) Natural flow: almost 2d characteristic

(b) Excited flow ($F^+ = 0.6, C_\mu = 50 \times 10^{-5}$) has a 3d characteristic

Figure 4: Streamlines showing the character of the flow above the flap.

easily be extracted using a stream line integration starting at a saddle into the inflow/outflow direction. See [SWTH07] for a discussion on how these lines can be compared with height ridges.

4 Results

In the following we apply our methods to analyze the impact of our active flow control technique at the airfoil. In particular, we study the influence of the actuation parameters *intensity* and *frequency*, but first we start with a basic description of the flow physics for the unexcited and excited case.

4.1 Unexcited Flow

The flow field of the *SCCH*-configuration without excitation is characterized by massive separation above the upper surface of the flap. The mean separation point is located close behind the flap leading edge, and downstream a large recirculation region occurs. The unsteady behaviour of separated flow is mainly governed by large vortices shed from the flap trailing edge that interact with the vortices generated in the shear layer between the recirculation region and the flow passing through the slot between main airfoil and flap nose. The unsteady structures are characterized by a two-dimensional behaviour (figure 4a).

4.2 Goal of the Excitation

It is the goal of the excitation to increase the lift by downsizing the recirculation zone and re-energizing it. To do so, we perturb the shear layer using a periodic excitation scheme as described in section 2.6. This increases the number of instabilities leading to a faster decay of the shear layer. These instabilities can be observed by means of vortex structures. A large, two-dimensional vortex binds a high amount of energy and causes less energy dissipation than smaller vortex structures with a three-dimensional characteristic. The smaller vortex structures help distributing the energy to the low-energy recirculation zone. Due to this the recirculation area becomes smaller.
Hence, the excitation has to influence the flow structures in the shear layer such that the vortices become smaller and have a three-dimensional characteristic. For this to happen, the parameters of the excitation have to be chosen carefully. In particular, the following parameters are of great importance:

- *Frequency*
  We have to influence the flow with a frequency that interacts with the natural frequencies of the flow. Only this way we can target the natural flow structures.
- *Intensity*
  The intensity of the excitation jet has to be strong enough to actually reach the shear layer.

In the following we study the influence of these two parameters on the vortex structures and the lift. While we can compute the lift directly, the vortex analysis helps us in understanding *why* a certain parameter combination exhibits the highest lift.

4.3 Parameter Study

In order to find an optimum excitation, simulations with different frequencies at $C_\mu = 50 \times 10^{-5}$ (which corresponds to the free stream impulse) are performed first. Different intensities are then simulated at the determined optimal frequency $F^+ = 0.6$. The excitation mode is equal to a sinusoidal blowing and suction.

4.3.1 Frequency of Air Injection

Figure 5a presents results of the excitation in the simulation with different frequencies. The diagram shows the difference of the lift coefficient relating to the unexcited case depending on excitation frequency. The largest lift can be found at a frequency of $F^+ = 0.6$. In this case the lift coefficient can be enhanced by 11% compared to the baseline simulation. In the range of strong gain in lift ($F^+ = 0.2 \ldots 0.5$) the infinite wing achieved the same change in lift at higher frequencies compared to the two-dimensional flow. At frequencies slightly higher than the optimal excitation frequency ($F^+ = 0.6$) the gain in lift decreases.
In figure 6 we show the results of our topology-based vortex analysis which has been applied to study the influence of the frequency of air injection. While we know *which* frequency yields the best lift, our main goal is to uncover the underlying physics: we want to know *why* a certain frequency yields higher lift than others.

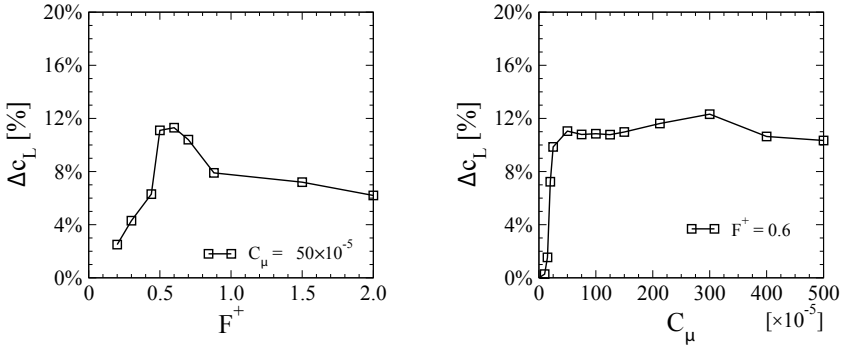

(a) Increase in the mean lift coefficient versus the non-dimensional excitation frequency

(b) Increase in the mean lift coefficient versus the non-dimensional excitation intensity

Figure 5: Numerical results of the excited flow.

Figure 6a indicates the setup: we want to achieve performance enhancements by controlling the flow separation at the rear flap using periodic air injection. The vortex structures have been extracted as topological separatrices of the pressure gradient and denote lines of minimal pressure. Figure 6c shows parts of the topological skeleton of the pressure gradient. A quantification of the separation lines based on pressure and a subsequent filtering of weak vortices has been applied. This allows us to concentrate on the most important information. The result is shown in figures 6d–f where the impact of the frequency of air injection onto the vortex structures can be studied. Note that this is a five-dimensional data set consisting of three spatial dimensions, time, and the frequency parameter dimension – the intensity is fixed. Raising the frequency causes a reduction of the lower vortex, which is a necessary condition for gaining lift. However, higher frequencies ($F^+ > 0.6$) are not beneficial to the lift. Using a visual comparison of the vortex structures at different frequencies, we found that new vortex structures are induced by the air injection itself. This has a negative effect on the pressure ratio and consequently on the lift. Especially at higher frequencies, the excitation dominates the natural flow structures and induces long-living, almost two-dimensional vortices in fast succession at the top of the rear flap (figure 6f). In contrast to this, the induced vortices at $F^+ = 0.6$ dissolve quickly and therefore, they are less influential.

We want to evaluate our analysis technique using a more traditional method. Figure 7 shows the trailing edge departure angle of the main airfoil in the unexcited case, which we define as the angle between the oncoming flow direction and the flow direction at the trailing edge. This angle is directly linked to the pressure distribution above the main airfoil: a larger angle indicates a higher pressure gradient which is a main trigger of increased lift. The second and third column of figure 7 show the trailing edge departure angle for the unexcited, optimally excited ($F^+ = 0.6$), and high-frequency excited flow ($F^+ = 2.0$). At $F^+ = 0.6$ (solid red line in 7b) we can observe a pronounced three-dimensionality in contrast to the other cases. This causes a higher dissemination of the excitation energy and

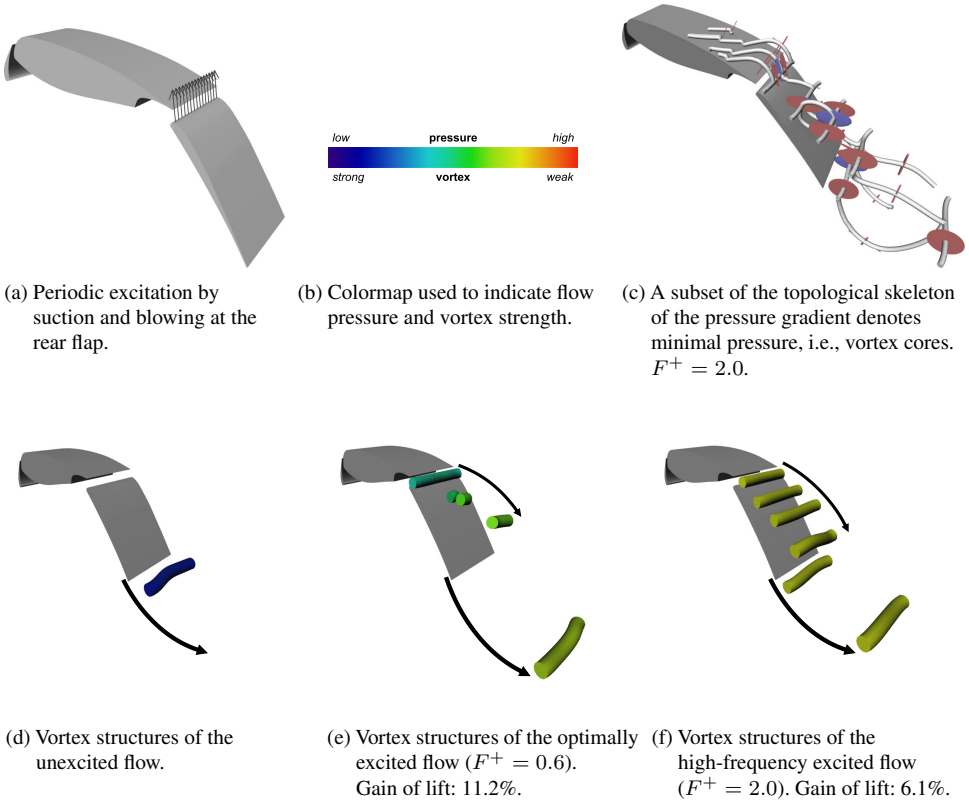

(a) Periodic excitation by suction and blowing at the rear flap.

(b) Colormap used to indicate flow pressure and vortex strength.

(c) A subset of the topological skeleton of the pressure gradient denotes minimal pressure, i.e., vortex cores. $F^+ = 2.0$.

(d) Vortex structures of the unexcited flow.

(e) Vortex structures of the optimally excited flow ($F^+ = 0.6$). Gain of lift: 11.2%.

(f) Vortex structures of the high-frequency excited flow ($F^+ = 2.0$). Gain of lift: 6.1%.

Figure 6: A topology-based vortex analysis of the flow around an airfoil elucidates the impact of an active flow control technique and explains why a high-frequency excitation leads to a smaller gain of lift.

inhibits the formation of strong vortex structures – as we already know from our vortex analysis, see figure 6e. At higher frequencies, the excitation dominates the natural flow and the departure angle is almost two-dimensional in spanwise direction similar to the unexcited case. This goes hand in hand with the observed vortex structures for these cases which are almost two-dimensional, too.
Our topology-based vortex analysis technique contributed to the physical understanding of the flow structures and was a substantial part of the optimal choice of parameters.

4.3.2 Intensity of Air Injection

At the optimal excitation frequency of $F^+ = 0.6$ we simulate 13 different excitation intensities of $C_\mu \cdot 10^5 = C'_\mu = 10, 15, 20, 25, 50, 75, 100, 125, 212, 300, 400, 500$. Figure 8 shows the result of our vortex analysis.
Excitation with low intensity ($C'_\mu = 10 \ldots 50$) leads to a strong increase in lift (max. 11%)

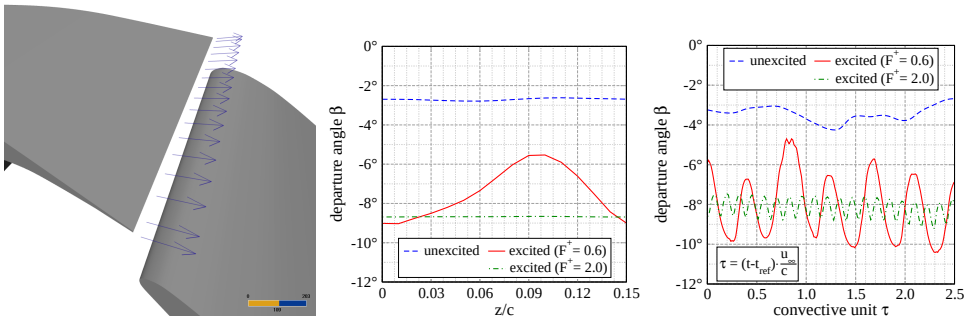

(a) trailing edge departure flow (b) snapshot (c) spanwise averaged

Figure 7: Our vortex analysis of different excitation frequencies could be evaluated successfully by examination of the trailing edge departure angle of the main airfoil (first column). The angle between these vectors and the oncoming flow direction is shown at a snapshot in the second column and spanwise averaged in the third. The dashed, solid and dotted lines denote the unexcited flow, $F^+ = 0.6$, $F^+ = 2.0$, respectively.

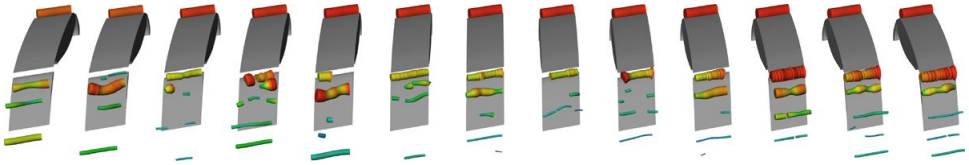

Figure 8: The intensity variation was performed on 13 different intensity values ranging from $C'_\mu = 10$ to $C'_\mu = 500$ (shown in increasing order from left to right). See figure 9 for a close-up.

(figure 5b). However, if C'_μ becomes larger than 50, the lift ceases to increase further. In general, the results for both excitation parameters show that the lift either cease to increase or begins to decrease slightly if the frequency or intensity exceeds a certain limit ($F^+ = 0.6$, $C'_\mu = 50$).

As in the frequency modulation, our topology-based vortex analysis helps in understanding those effects: At a low intensity of $C'_\mu = 10$, the excitation jet is too weak to perturb the shear layer significantly, see figure 9a. This changes at higher intensities. At $C'_\mu = 20$ (figure 9b) and $C'_\mu = 50$ (figure 9c) three-dimensional vortex structures are produced as expected by the perturbation of the shear layer. However, at $C'_\mu = 500$, the excitation is so intense that the excitation jet penetrates through the shear layer and a significant part of the energy is absorbed by the free stream. This results in a large, excitation induced vortex with a very short life cycle (figure 9d). As only parts of the energy can be used to destroy the shear layer, the downstream vortices keep much of their two-dimensional characteristics. Furthermore, $C'_\mu = 500$ is 10 times higher than in the $C'_\mu = 50$. Although the effectivity is comparable, the excitation with $C'_\mu = 50$ is much more efficient.

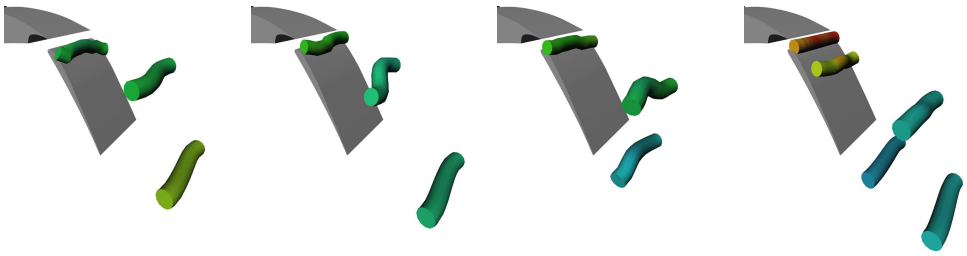

(a) $C'_\mu = 10$. (b) $C'_\mu = 20$. (c) $C'_\mu = 50$. (d) $C'_\mu = 500$.

Figure 9: Topology-based vortex analysis of the intensity variation at four selected intensities. At intensities of $C'_\mu = 20$ and $C'_\mu = 50$ the structures are three-dimensional, whereas at lower and higher intensity, the structures have a two-dimensional characteristic. At $C'_\mu = 500$, a strong excitation-induced vortex is created at the top of the rear flap.

5 Conclusions

We examined a high-dimensional flow data set around an airfoil which totals in over 200GB of data. This 3D time-dependent flow depends on two additional parameters introduced by the periodic blowing and suction: frequency and intensity of air injection. Using a topology-based vortex analysis we were able to identify the influence of parameter variations on the flow field and elucidated the underlying physics.

Acknowledgments

We thank Bernd R. Noack for the fruitful discussions. All visualizations in this paper have been created using AMIRA – a system for advanced visual data analysis [SWH05b] (see `http://amira.zib.de/`).

References

[BS95] D.C. Banks and B.A. Singer. A predictor-corrector technique for visualizing unsteady flow. *IEEE Transactions on Visualization and Computer Graphics*, 1(2):151–163, 1995.

[Ebe96] D. Eberly. *Ridges in Image and Data Analysis*. Kluwer Acadamic Publishers, Dordrecht, 1996.

[EHNP03] H. Edelsbrunner, J. Harer, V. Natarajan, and V. Pascucci. Morse-smale complexes for piecewise linear 3-manifolds. In *Proc. 19th Sympos. Comput. Geom. 2003*, pages 361 – 370, 2003.

[GeH01] M. Gad-el Hak. Flow control: The future. *Journal of Aircraft*, 38(3), 2001.

[HH91] J. Helman and L. Hesselink. Visualizing vector field topology in fluid flows. *IEEE Computer Graphics and Applications*, 11:36–46, May 1991.

[HJ97] A.A. Hassan and R.D. Janakiram. Effects of zero-mass synthetic jets on the aerodynamics of the NACA-0012 airfoil. *AIAA Paper 97-2326*, 1997.

[Hun87] J.C.R Hunt. Vorticity and vortex dynamics in complex turbulent flows. *Proc CANCAM, Trans. Can. Soc. Mec. Engrs*, 11:21, 1987.

[JH95] J. Jeong and F. Hussain. On the identification of a vortex. *J. Fluid Mechanics*, 285:69–94, 1995.

[KKE05] K. Kaepernick, L. Koop, and K. Ehrenfried. Investigation of the unsteady flow field inside a leading edge slat cove. In *11th AIAA/CEAS Aeroacoustics Conference (26th Aeroacoustics Conference), Monterey, CA, USA*, 2005.

[Koo05] L. Koop. *Aktive und Passive Strömungsbeeinflussung zur Reduzierung der Schallabstrahlung an Hinterkanntenklappen von Tragflügeln*. PhD thesis, Technische Universität Berlin, 2005.

[MCML89] D.V. Maddalon, F.S. Collier, L.C. Montoya, and C.K. Land. Transition flight experiments on a swept wing with suction. *AIAA Paper 89-1893*, 1989.

[Mil63] John Willard Milnor. *Morse Theory*, volume 51 of *Annals of Mathematics Studies*. Princeton, NJ, USA, 1963.

[MK97] H. Miura and S. Kida. Identification of tubular vortices in turbulence. *J. Physical Society of Japan*, 66(5):1331–1334, 1997.

[MSDS] H. Meuer, E. Strohmaier, J. Dongarra, and H. Simon. Top500 supercomputer sites. http://www.top500.org/.

[PR99] R. Peikert and M. Roth. The parallel vectors operator - a vector field visualization primitive. In *Proc. IEEE Visualization 99*, pages 263–270, 1999.

[PVH+02] F.H. Post, B. Vrolijk, H. Hauser, R.S. Laramee, and H. Doleisch. Feature extraction and visualisation of flow fields. In *Proc. Eurographics 2002, State of the Art Reports*, pages 69–100, 2002.

[RM00] J.B.T.M. Roerdink and A. Meijster. The watershed transform: Definitions, algorithms and parallelization strategies. *Fundamenta Informaticae*, 41(1-2):187–228, 2000.

[RP98] M. Roth and R. Peikert. A higher-order method for finding vortex core lines. In D. Ebert, H. Hagen, and H. Rushmeier, editors, *Proc. IEEE Visualization '98*, pages 143–150, Los Alamitos, 1998. IEEE Computer Society Press.

[RT96] T. Rung and F. Thiele. Computational modelling of complex boundary-layer flows. In *9th Int. Symp. on Transport Phenomena in Thermal-Fluid Engineering, Singapore*, 1996.

[SGT04] M. Schatz, B. Günther, and F. Thiele. Computational modelling of the unsteady wake behind gurney-flaps. *AIAA Paper 2004-2417*, 2004.

[SH95] D. Sujudi and R. Haimes. Identification of swirling flow in 3D vector fields. Technical report, Department of Aeronautics and Astronautics, MIT, 1995. AIAA Paper 95-1715.

[SRE05] S. Stegmaier, U. Rist, and T. Ertl. Opening the Can of Worms: An Exploration Tool for Vortical Flows. In *Proc. IEEE Visualization 05*, pages 463–470. IEEE, 2005.

[SWH05a] J. Sahner, T. Weinkauf, and H.-C. Hege. Galilean invariant extraction and iconic representation of vortex core lines. In K. Joy K. Brodlie, D. Duke, editor, *Proc. Eurographics / IEEE VGTC Symposium on Visualization (EuroVis '05)*, pages 151–160, Leeds, UK, June 2005.

[SWH05b] D. Stalling, M. Westerhoff, and H.-C. Hege. Amira: A highly interactive system for visual data analysis. *The Visualization Handbook*, pages 749–767, 2005.

[SWTH07] J. Sahner, T. Weinkauf, N. Teuber, and H.-C. Hege. Vortex and strain skeletons in eulerian and lagrangian frames. *IEEE Transactions on Visualization and Computer Graphics*, 13(5):980–990, September - October 2007.

[TWHS03] H. Theisel, T. Weinkauf, H.-C. Hege, and H.-P. Seidel. Saddle connectors - an approach to visualizing the topological skeleton of complex 3D vector fields. In *Proc. IEEE Visualization 2003*, pages 225–232, 2003.

[WSTH07] T. Weinkauf, J. Sahner, H. Theisel, and H.-C. Hege. Cores of swirling particle motion in unsteady flows. *IEEE Transactions on Visualization and Computer Graphics (Proceedings Visualization 2007)*, 13(6):1759–1766, November - December 2007.

[Wyg04] I. Wygnanski. The variables affecting the control separation by periodic excitation. *AIAA Paper 2004-2505*, 2004.